Electronic Supplementary Material (ESI) for ChemComm.
This journal is © The Royal Society of Chemistry 2019

Electronic Supplementary Information (ESI)

Crystal-to-crystal interconversion of open and closed dicopper(II) paddle-wheels in a heterotrimetallic coordination polymer

Hayato Ohwaki, Nobuto Yoshinari, and Takumi Konno*

Department of Chemistry, Graduate School of Science, Osaka University, Toyonaka, Osaka 560-0043 (Japan)

konno@chem.sci.osaka-u.ac.jp

Experimental Section

A. Preparation of [$Au_2Pd(dppm)(D\text{-}pen)_2$] ([1]).

To a pale yellow solution containing 1.15 g (986 μmol) of [$Au_2(dppm)(D\text{-}Hpen)_2]\cdot 5H_2O$ [13] in 100 mL of ethanol, 0.22 g (986 μmol) of $Pd(OAc)_2$ was added. The mixture was stirred at room temperature for 3 h, which gave a yellow solution. The yellow solution was evaporated to dryness, and the yellow residue was dissolved in 40 mL of ethanol/water (1:1). The yellow solution was allowed to stand at room temperature for 6 days. After filtration to remove a small amount of yellow crystalline film, 100 μL of EtOH was added to the resulting yellow filtrate. The mixture was allowed to stand at room temperature for 2 days, which gave yellow block crystals ([**1**]$\cdot 8H_2O$). One of the crystals was used for the single-crystal X-ray analysis. Yield: 0.92 g (71%). Anal. Found: C, 31.78; H, 4.08; N, 2.11%. Calcd for [$Au_2Pd(dppm)(D\text{-}pen)_2]\cdot 8H_2O$ = $C_{35}H_{56}N_2O_{12}P_2S_2Au_2Pd$: C, 31.77; H, 4.27; N, 2.12%. IR spectrum (cm^{-1}, KBr disk): 1605 (ν_{COO}), 1437 (ν_{Ph}), 1102, and 786-690 (ν_{P-Ph}). ^1H NMR spectrum (ppm from TMS, methanol-d_4): δ 1.54 (s, 6H), 1.75 (s, 6H), 3.39 (s, 2H), 7.38-7.77 (m, 20H). ^{31}P NMR spectrum (ppm from 85% H_3PO_4, methanol-d_4): δ 33.2 (s).

B. Preparation of [$Cu_2(H_2O)_4\{Au_2Pd(dppm)(D\text{-}pen)_2\}_2](NO_3)_4$ ([2]$(NO_3)_4$).

To a yellow solution containing 60 mg (45.3 μmol) of [**1**]$\cdot 8H_2O$ in 2 mL of ethanol, 0.1 M $Cu(NO_3)_2$ (2.0 mL, 2.0 mmol) in a mixture of water/ethanol (v/v = 4/1) was added, which gave a blue green solution. The solution was carefully evaporated in a closed desiccator at room temperature for 6 days, which gave green block crystals ([**2**]$(NO_3)_4\cdot 4H_2O$). One of the crystals was used for the single-crystal X-ray analysis. Yield: 49 mg (75%). Anal. Found: C, 29.33; H, 3.34; N, 3.89%. Calcd for [$Cu_2(H_2O)_4\{Au_2Pd(dppm)(D\text{-}pen)_2\}_2](NO_3)_4\cdot 4H_2O$ = $C_{70}H_{96}N_8O_{28}P_4S_4Au_4Pd_2$: C, 29.22; H, 3.36; N, 3.89%. IR spectrum (cm^{-1}, KBr disk): 1650 and 1605 (ν_{COO}), 1437 (ν_{Ph}), 1385 (ν_{NO3}), 1102, and 789-690 (ν_{P-Ph}).

C. Preparation of [$Cu_2(H_2O)_2\{Au_2Pd(dppm)(D\text{-}pen)_2\}_2](NO_3)_4$ ([3]$(NO_3)_4$).

Green crystals of [**2**]$(NO_3)_4\cdot 4H_2O$ were dried under 0.6 kPa at room temperature for 15 min to give dehydrated crystals ([**3**]$(NO_3)_4\cdot 3H_2O$). During this treatment, cracks occurred in the crystals. One of the single-crystal domains was used for the single-crystal X-ray analysis, from which its formula was estimated to be [$Cu_2(H_2O)_2\{Au_2Pd(dppm)(D\text{-}pen)_2\}_2](NO_3)_4\cdot 3H_2O$, together with the water adsorption analysis (Figure S11). The elemental analysis of [**3**]$(NO_3)_4\cdot 3H_2O$ as well as measurement of its IR spectrum could not be carried out because crystals of [**3**]$(NO_3)_4\cdot 3H_2O$ quickly adsorb water molecules under ambient conditions to be revert back to [**2**]$(NO_3)_4\cdot 4H_2O$.

D. Physical Measurements.

The IR spectra were recorded on a JASCO FT/IR-4100 spectrometer using KBr disks at room temperature. The ^1H and ^{31}P NMR spectra were measured on a JEOL ECA-500 NMR spectrometer at room temperature using tetramethylsilane (TMS, δ 0.0 ppm) as the internal standard for ^1H NMR and triphenyl phosphate (δ –17.6 ppm) as the external standard for ^{31}P NMR. The elemental analyses (C, H, N) were performed using a YANACO CHN coder MT-5

or MT-6. TG-DTA measurements were performed on a SHIMADZU DTG60 under N_2 gas flow (50 mL/min) using Al_2O_3 as a reference with the scan rate of 5.0 ºC/min. The X-ray fluorescence spectrometry was performed on a SHIMADZU EDX-720 spectrometer. The sorption isotherms for H_2O were performed on a BELSORP-max volumetric adsorption instrument. The powder X-ray diffraction patterns were recorded under controlled temperature in the transmission mode [synchrotron radiation λ = 1.0 Å; 2θ range = 2–78˚; step width = 0.01˚; data collection time = 1 min] on a diffractometer equipped with a MYTHEN microstrip X-ray detector (Dectris Ltd.) at the SPring-8 BL02B2 beamline. The crystals were loaded into a glass capillary tube (diameter = 0.3 mm). The sample was rotated during the measurements. The powder simulation patterns were generated from the single-crystal X-ray structures using Mercury 3.9. The crystals for vacuum-condition measurements were loaded into a glass capillary tube (diameter = 0.5 mm), and the glass capillary tube was connected with a rotary pump under controlled pressure monitored by a Pirani vacuum gauge. The sample was oscillated during the measurements.

E. Magnetic susceptibility measurements.

Magnetic susceptibility data were collected for crystalline samples on a QUANTUM DESIGN MPMS SQUID magnetometer at temperatures ranging from 2 to 300 K under an applied magnetic field of 5000 Oe. The magnetic susceptibility data were analyzed by a least-square fitting based on the Van Vleck model considering temperature independent paramagnetism (T.I.P), the spin coupling parameter (2J), and the molar ratio of paramagnetic impurity (α).

$$\chi_M T = \frac{N_A {\mu_B}^2 g^2}{3k} \frac{6}{1+\exp(-2J/kT)}(1-\alpha) + \frac{N_A {\mu_B}^2 g^2}{4k} 2\alpha + T.I.P. \times T$$

The original data and simulated curves are illustrated in the same chart in Figure 3. The magnetic susceptibility data are summarized in Table S2.

F. X-ray diffraction analysis.

The single-crystal X-ray diffraction measurement for [**1**] was performed on a RIGAKU FR-E Superbright rotating-anode X-ray source with Mo-target (λ = 0.71075 Å) equipped with a RIGAKU RAXIS VII imaging plate as a detector at 200 K. The intensity data were collected by the ω scan mode and were corrected for Lorentz polarization. Empirical absorption corrections were also applied. The single-crystal synchrotron radiation X-ray diffraction measurement for [**2**]$(NO_3)_4$ was carried out at the BL02B1 beamline in Spring-8 at 100 K (λ = 0.7 Å). The intensity data were collected by the ω scan mode and were corrected for Lorentz polarization. Empirical absorption corrections were also applied. The single-crystal synchrotron radiation X-ray diffraction measurement for [**3**]$(NO_3)_4$ was carried out on an ADSC Q210 CCD area detector with synchrotron radiation at the 2D beamline in the Pohang Accelerator Laboratory (PAL) at 100 K (λ = 0.63 Å). The diffraction images were processed by using HKL3000.

The structures of the compounds were solved by direct methods using SHELXS-2014.[S1] The structural refinements were carried out using full matrix least-squares (SHELXL-2014).[S1] Hydrogen atoms were included in the calculated positions, except for those of the water molecules. The high R_{int} value of 0.175 for crystal [**2**]$(NO_3)_4$ is most likely due to the twinning

of crystal.

The crystal data are summarized in Tables S1 and S3.

References.

(S1) G. M. Sheldrick, *Acta Cryst.*, 2008, **A64**, 112.

2. Figures

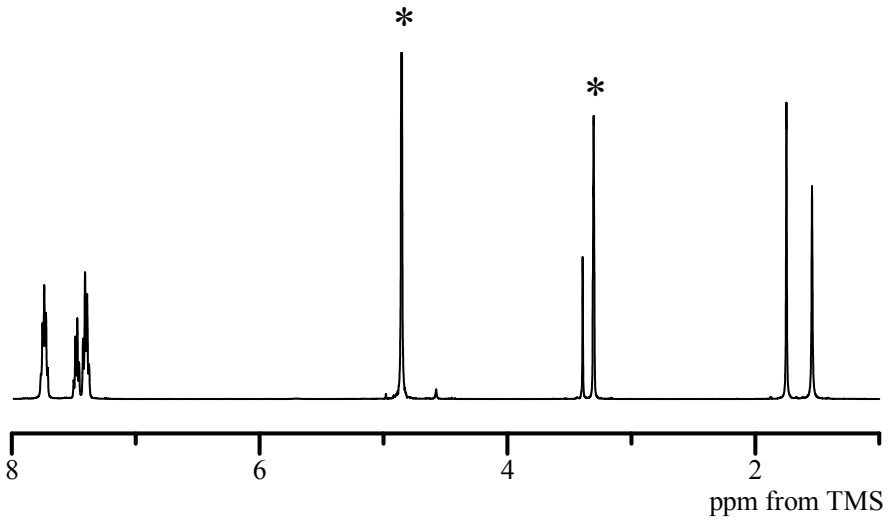

Figure S1. ^{1}H NMR spectrum of [**1**] in methanol-d_4. The spectrum was measured at 298 K. (*) denotes the signals from solvents. The signals corresponding to the NH_2 group of D-pen and the CH_2 group of dppm were not observed in the spectrum, most likely due to the rapid H/D exchange for these protons.

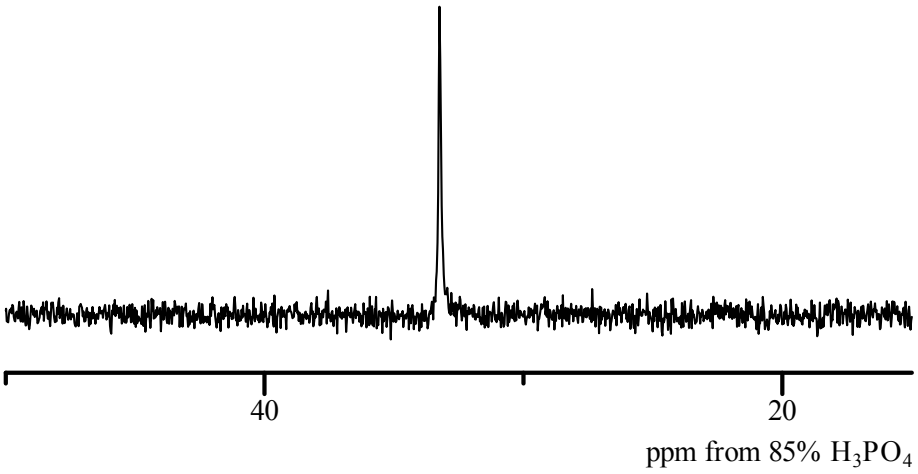

Figure S2. ^{31}P NMR spectrum of [**1**] in methanol-d_4. The spectrum was measured at 298 K.

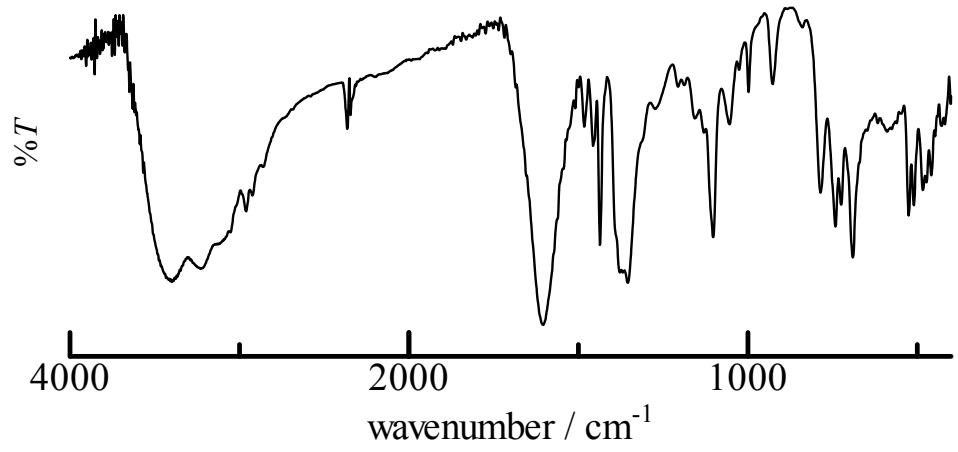

Figure S3. The IR spectrum of [**1**].

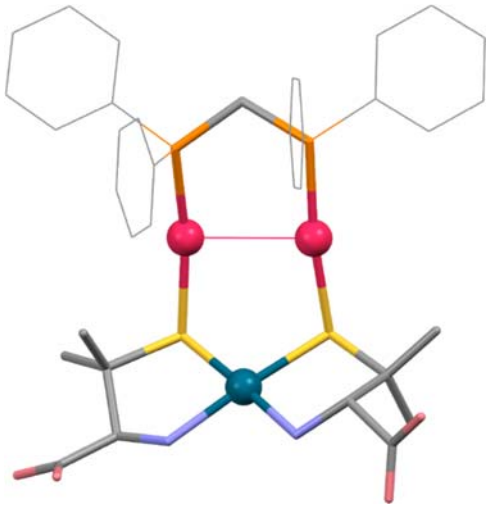

Figure S4. A perspective view of the molecular structure of [**1**]. Color code: Au, pink; Pd, blue-green; S, yellow; O, pink; N, blue; and C, gray. H atoms were omitted for clarity.

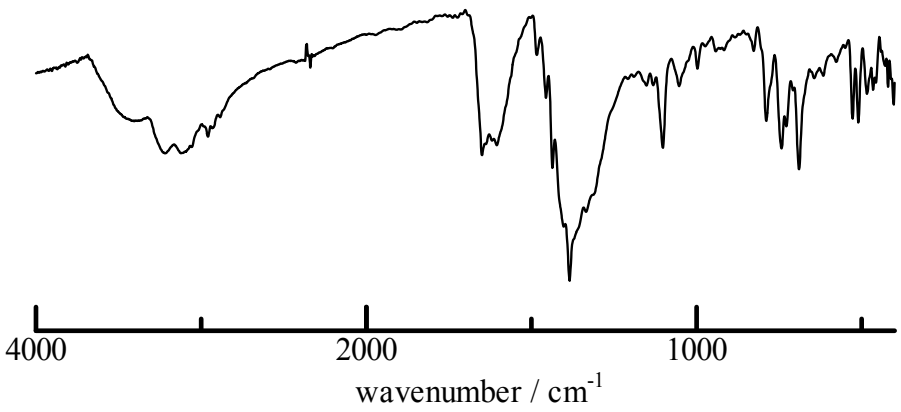

Figure S5. The IR spectrum of [**2**]$(NO_3)_4$.

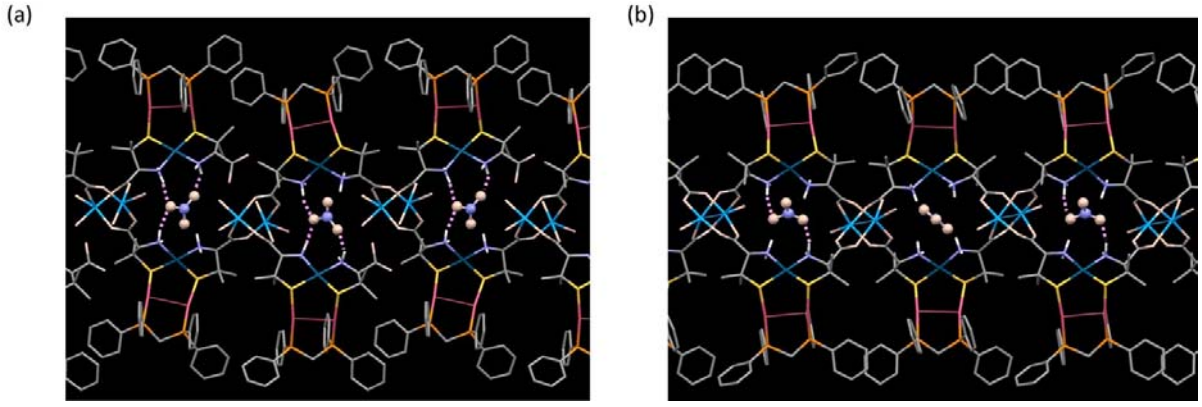

Figure S6. Perspective views showing the environments around nitrate ions accommodated inside the 1D coordination polymers in (a) [**2**]$(NO_3)_4$ and (b) [**3**]$(NO_3)_4$. Pink dashed lines represent hydrogen bonds. All H atoms except for amine groups were omitted for clarity.

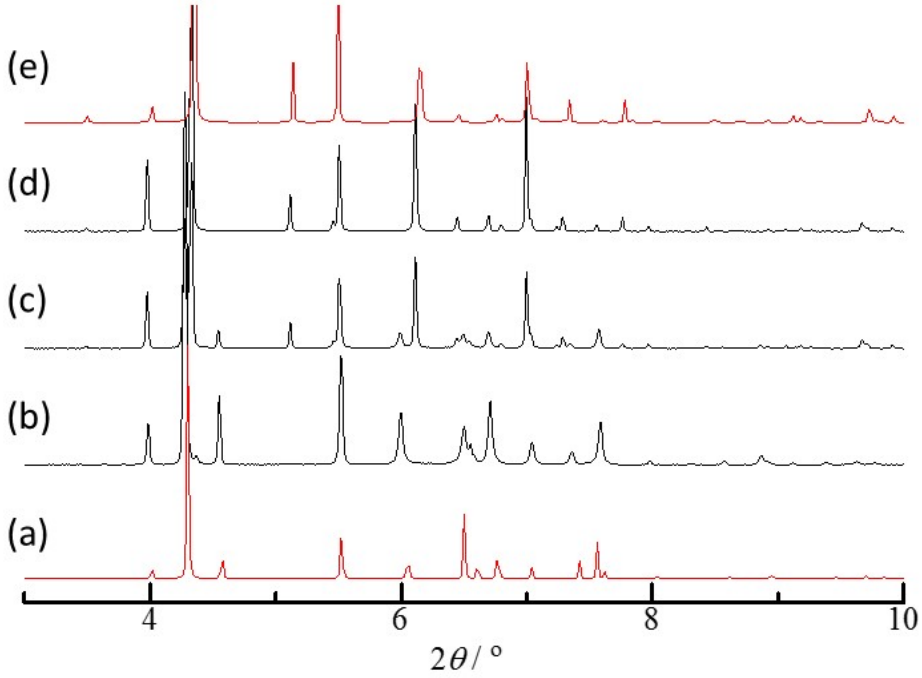

Figure S7. (a) The simulated PXRD pattern of [**3**](NO$_3$)$_4$, the observed PXRD patterns of (b) a freshly prepared sample of [**3**](NO$_3$)$_4$, (c) a sample after exposure to humidified air for 3 min, (d) a sample after exposure to humidified air for 8 min, and (e) the simulated PXRD pattern of [**2**](NO$_3$)$_4$.

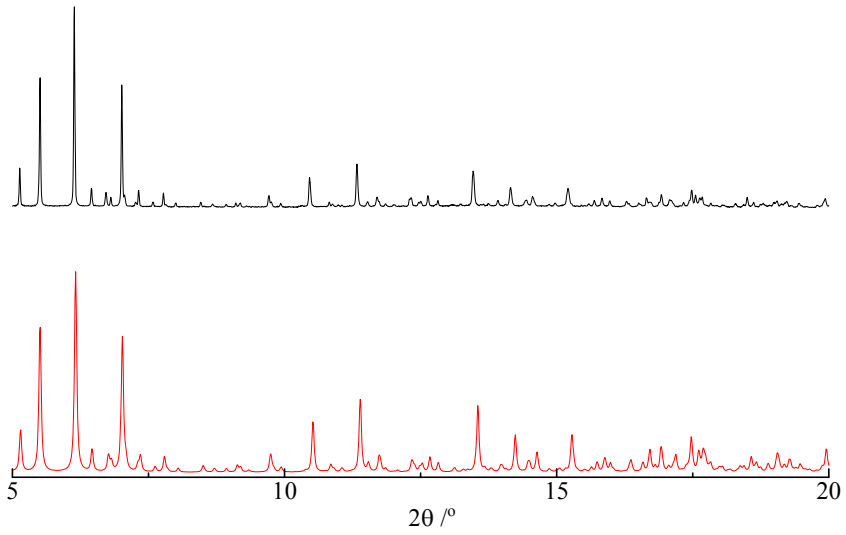

Figure S8. Simulated (red) and observed (black) powder X-ray diffraction patterns of [**2**](NO$_3$)$_4$.

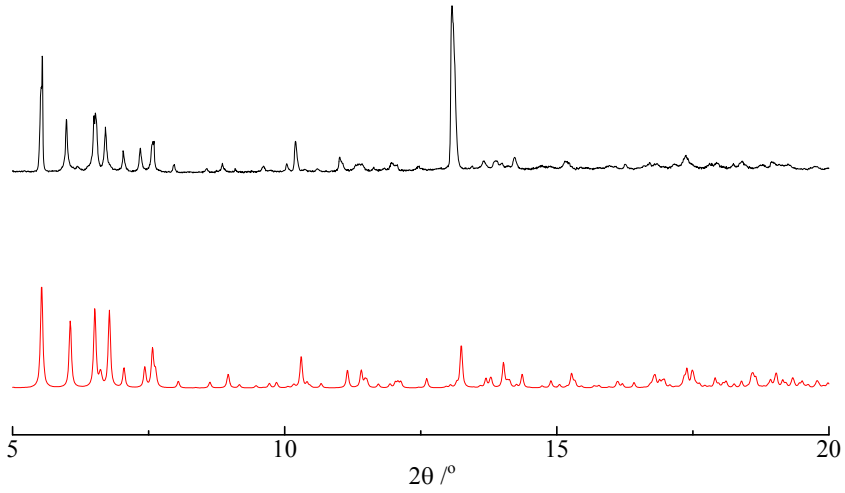

Figure S9. Simulated (red) and observed (black) powder X-ray diffraction patterns of [**3**](NO$_3$)$_4$.

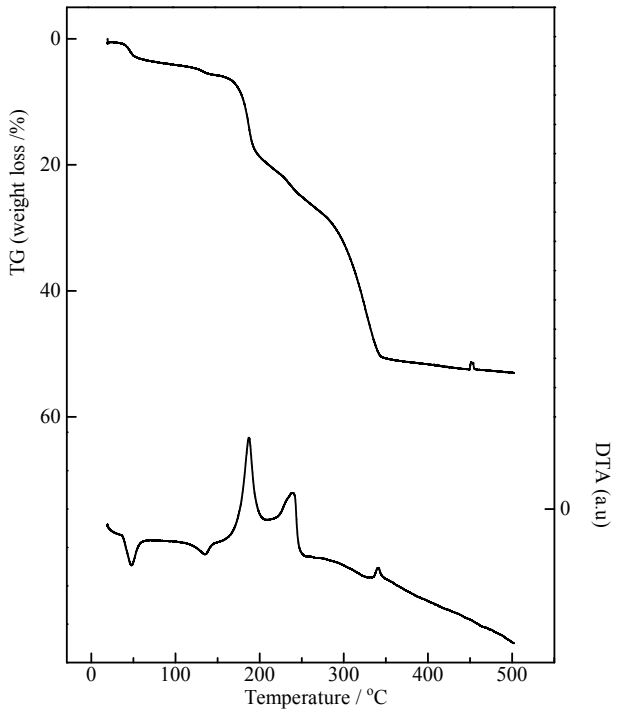

Figure S10. TG/DTA curves of [**2**](NO$_3$)$_4$.

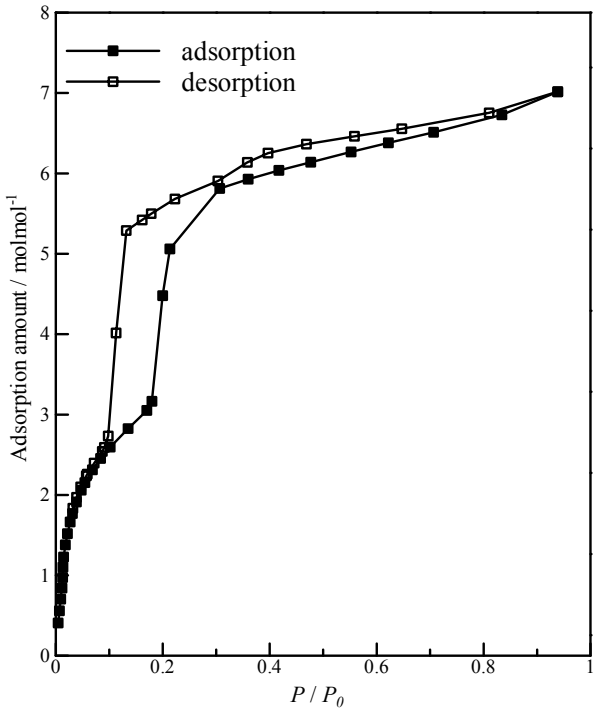

Figure S11. H_2O vapor adsorption and desorption isotherms at 298 K for the activated sample of [**2**]$(NO_3)_4$. The two-step hysteresis loop supports the chemical sorption of three water molecules in the framework of [**2**]$(NO_3)_4$.

(a)

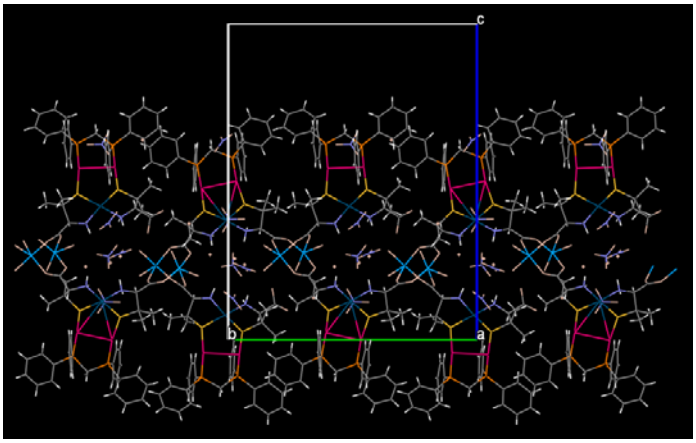

(b)

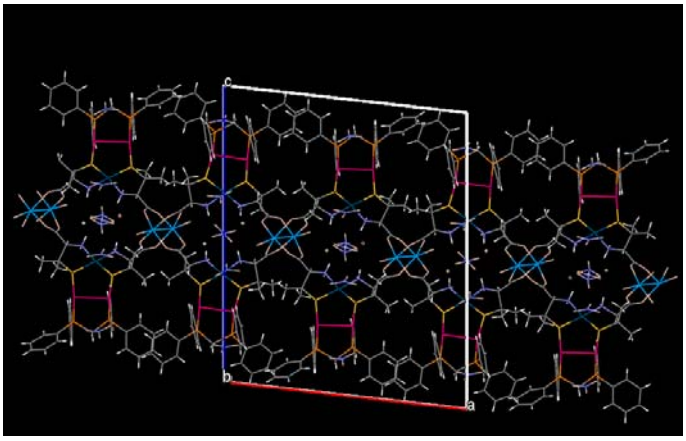

Figure S12. Packing views of (a) [**2**]$(NO_3)_4$ from *a* axis and (b) [**3**]$(NO_3)_4$ from *b* axis, emphasizing the transformation of crystal lattice.

Table S1. Effective hydrogen-bonding parameters between amine groups and nitrate ions.

parameter	N···O/ Å	N-H···O /°
	[**2**](NO$_3$)$_4$	
N1 H1 O13	2.87(3)	168.2
N2 H4 O15	3.01(4)	154.5
N4 H44 O13	2.96(3)	164.4
	[**3**](NO$_3$)$_4$	
N4 H43 O21	2.84(3)	165.1

Table S2. Fitting parameters obtained from the magnetic data analysis.

parameter	[**2**](NO$_3$)$_4$ increasing	[**2**](NO$_3$)$_4$ decreasing	[**3**](NO$_3$)$_4$
g	2.1	2.1	2.1
$2J$ / J	-114(1)	-308(1)	-288(1)
T.I.P / cm^{3}mol^{-1}	$2.8(1) \times 10^{-4}$	$3.7(1) \times 10^{-4}$	$3.3(1) \times 10^{-4}$
α	0.02(1)	0.04(1)	0.03(1)

Table S3. Crystallographic data of compounds.

	[**1**]·11.5H_2O·0.25EtOH	[**2**]$(NO_3)_4$·4H_2O	[**3**]$(NO_3)_4$·3H_2O
λ (Å)	0.71073	0.7002	0.6300
Formula	$C_{142}H_{258}Au_8N_8O_{63}P_8Pd_4S_8$	$C_{70}H_{96}Au_4Cu_2N_8O_{28}P_4Pd_2S_4$	$C_{70}H_{90}Au_4Cu_2N_8O_{25}P_4Pd_2S_4$
Color, form	Yellow, block	Green, block	Green, block
M_w	5591.12	2877.41	2823.36
Crystal system	Monoclinic	Orthorhombic	Monoclinic
Space group	$P2_1$	$P2_12_12_1$	$I2$
a (Å)	16.2767(3)	16.8393(17)	20.842(4)
b (Å)	37.3828(7)	20.715(2)	17.342(4)
c (Å)	16.9637(3)	26.283(3)	25.184(5)
α (°)	90	90	90
β (°)	99.887(7)	90	96.43(3)
γ (°)	90	90	90
V (Å^3)	10168.6(4)	9167.9(17)	9045(4)
Z	2	4	4
T (K)	200(2)	100(2)	100(2)
R_{int}	0.0548	0.1746	0.0928
F(000)	5468	5544	5424
ρ calcd (g cm^{-3})	1.826	2.085	2.073
μ (Mo Kα) (mm^{-1})	6.313	7.126	5.490
Crystal size (mm^3)	0.16×0.16×0.16	0.06×0.03×0.03	0.05×0.04×0.03
Limiting indices	$-20 \le h \le 18$	$-21 \le h \le 21$	$-32 \le h \le 32$
	$-48 \le k \le 48$	$-24 \le k \le 26$	$-27 \le k \le 27$
	$-22 \le l \le 21$	$-34 \le l \le 33$	$-39 \le l \le 39$
$R1$ ($I > 2\sigma(I)$)[a)]	0.0576	0.0807	0.0625
w$R2$ (all data)[b)]	0.0809	0.1742	0.1536
GOF	1.021	0.924	0.873
Flack	0.051(4)	-0.017(10)	0.010(5)

a) $R1 = \Sigma||F_o|-|F_c|| \,/\, \Sigma|F_o|$.

b) $wR2 = [\Sigma(w(F_o^2-F_c^2)^2) \,/\, \Sigma w(F_o^2)^2]^{1/2}$.